

Synchrotron X-ray scattering and reflectivity studies of the structure of low dielectric constant SiOCH thin films prepared from bistrimethylsilylmethane by chemical vapor deposition

Kyuyoung Heo,^{a,‡} Kyoung Suk Oh,^{b,‡} Jinhwan Yoon,^a Kyeong Sik Jin,^a Sangwoo Jin,^a Chi Kyu Choi^{b,*} and Moonhor Ree^{a,*}

^aDepartment of Chemistry, Pohang Accelerator Laboratory, National Research Laboratory for Polymer Synthesis and Physics, Center for Integrated Molecular Systems, Polymer Research Institute, and BK School of Molecular Science, Pohang University of Science and Technology (POSTECH), Pohang 790-784, Republic of Korea, and ^bNano-Thin Film Materials Laboratory, Department of Physics, Cheju National University, Jeju 690-756, Republic of Korea. Correspondence e-mail: cckyu@cheju.ac.kr, ree@postech.edu

Quantitative, non-destructive grazing-incidence X-ray scattering and specular X-ray reflectivity analysis with synchrotron radiation sources, along with spectroscopic ellipsometry analysis, were successfully used to characterize a series of low dielectric constant, nanoporous SiOCH dielectric thin films with nanometre-scale thicknesses prepared by radio-frequency inductively coupled plasma chemical vapor deposition of bistrimethylsilylmethane precursor and oxygen gas at various flow rate ratios followed by annealing at 298, 473, 573 or 673 K. These analyses provided important information on the structures and properties of the nanoporous films. The average size of the nanopores generated in each film was 3.07 nm in radius or less, depending on the process conditions. The film electron densities ranged from 414 to 569 nm⁻³, the refractive indices ranged from 1.434 to 1.512 at 633 nm wavelength, and the porosities ranged from 16.1 to 38.9%. Collectively, the present findings show that SiOCH thin films of the type reported here are suitable for use as low dielectric constant interdielectric layer materials in the fabrication of advanced integrated circuits.

© 2007 International Union of Crystallography
Printed in Singapore – all rights reserved

1. Introduction

Efforts to increase the density and performance of advanced micro-electronic devices, as well as to reduce costs, have led to decreases in the active device dimensions of integrated circuits (ICs) through the use of dense conductor-line wiring in multilevel structures and smaller features. However, shrinking the device feature size causes severe resistance–capacitance coupling problems, including signal delay and crosstalk noise between the metal interconnects. This signal delay and noise, as well as power consumption, depend critically on the dielectric constant (k) of the interdielectric layers. Thus, much effort has been devoted to developing new low- k dielectric materials to replace the current workhorse dielectrics, namely silicon dioxide ($k = 3.9$ – 4.3) and silicon nitride ($k = 6.0$ – 7.0) (Azooz *et al.*, 2003; Bolze *et al.*, 2001; Maex *et al.*, 2003; Maier, 2001; Morgen *et al.*, 2000; Kim *et al.*, 2005; Oh *et al.*, 2003; Lee, Oh, Hwang *et al.*, 2005; Lee, Oh, Yoon *et al.*, 2005; Lee, Park, Hwang *et al.*, 2005; Lee, Yoon *et al.*, 2005; Ree *et al.*, 2006; Yoon *et al.*, 2006).

Recently, thin films of silicon oxide containing alkyl groups (SiOCH) have been intensively studied as alternative dielectrics on account of their low k values, good mechanical strengths, and high thermal stabilities. To date, the preparation of SiOCH dielectrics by plasma-enhanced chemical vapor deposition (PECVD) has been examined using various silane precursors, including trimethylsilane (Loboda *et al.*, 1998), tetramethylsilane (Grill & Patel, 1999),

hexamethyldisiloxane (Shirafuji *et al.*, 1999), and bistrimethylsilylmethane (BTMSM) (Oh *et al.*, 2004; Kim *et al.*, 2003; Jun *et al.*, 2003). The resulting SiOCH dielectric films were extensively studied in terms of their chemical compositions and chemical, physical and dielectric properties (Grill & Patel, 1999; Jun *et al.*, 2003; Kim *et al.*, 2003; Loboda *et al.*, 1998; Oh *et al.*, 2004; Shirafuji *et al.*, 1999). However, only a small number of studies on SiOCH dielectrics have examined the film structure, knowledge of which is critical to understanding the dielectric, physical and mechanical properties (Grill *et al.*, 2003; Takahashi *et al.*, 2003; Yu *et al.*, 2003).

In the present study, we prepared SiOCH dielectric films on silicon substrates from mixtures of BTMSM and oxygen gas with various compositions by a radio-frequency inductively coupled plasma chemical vapor deposition (ICPCVD) process, and subsequently annealed the films for 30 min in a vacuum at 473, 573, or 673 K. The resulting dielectric films were quantitatively investigated using grazing-incidence X-ray scattering (GIXS) and specular X-ray reflectivity (XR) with synchrotron radiation sources. This combined GIXS and XR analysis provided details on the film structure, electron density, and electron density gradient along the thickness direction, as well as the pore shape and size distribution in the film.

2. Experiment

SiOCH films were prepared on pre-cleaned p -type Si(100) substrates by radio-frequency (13.56 MHz) ICPCVD of a mixture of BTMSM

[‡] K. Heo and K. S. Oh contributed equally to this work.

and O₂. In the deposition process, the silicon substrates were in a floating potential without heating, and the inductively coupled plasma was generated by means of a three-turn coil, which was set around a quartz tube. A base pressure of 1.33×10^{-4} Pa was reached before each deposition. The BTMSM precursor (410 K boiling point and 232 K melting point at standard atmospheric pressure) was vaporized and carried into the reaction chamber with the aid of inert argon gas from a thermostatic bubbler that was maintained at 313 K. To prevent any condensation of the vaporized BTMSM, all of the gas delivery lines were maintained at 313 K. The O₂ and BTMSM gases were introduced into the reaction chamber through a mass flow controller (MFC), and the discharge pressure was measured with a Baratron gauge and kept at about 33.33 Pa. The flow rate ratio [R_{fr} (%) = BTMSM/(BTMSM + O₂)], which is a measure of the composition of the BTMSM/O₂ mixture, was varied from 45 to 85% while maintaining a constant total gas flow rate of 40 s.c.c.m. (standard cm³ min⁻¹). The plasma density and electron temperature at an RF power of 300 W were 1012 cm⁻³ and 1.6 eV, respectively. The deposited films were further annealed for 30 min in a vacuum at 473, 573 or 673 K. The dielectric films obtained were determined to have thicknesses in the range 70–300 nm by spectroscopic ellipsometry.

GIXS measurements were carried out at the 4C1 and 4C2 beamlines (Bolze *et al.*, 2002, 2001; Yu *et al.*, 2005) of the Pohang Accelerator Laboratory (PAL) (Ree & Ko, 2005). The sample-to-detector distance was 2156 mm, and an X-ray wavelength $\lambda = 0.154$ nm and a two-dimensional (2D) charge-coupled detector (CCD) (Roper Scientific, Trenton, NJ) were used. Samples were mounted on a home-made z-axis goniometer equipped with a vacuum chamber. The incidence angle α_i of the X-ray beam was set at 0.20°, which is between the critical angles of the films and the silicon substrate ($\alpha_{c,f}$ and $\alpha_{c,s}$). Scattering angles were corrected for the variations in the positions of the X-ray beams reflected from the silicon substrate interface with changes in the incidence angle α_i and by a pre-calibrated copolymer, polystyrene-*b*-polyethylene-*b*-polybutadiene-*b*-polystyrene. Aluminium foil strips were employed as semi-transparent beam stops because the specular reflection from the substrate was much more intense than the GIXS near the critical angle.

Specular XR data were measured at the 3C2 beamline (Park *et al.*, 1995) of PAL. Samples were mounted on a Huber four-circle goniometer, and a scintillation counter with an enhanced dynamic range (Bede Scientific, EDR) was used as a detector. The horizontal beam size at the sample position was *ca.* 2 mm, and the full width at half-maximum of the direct beam profile measured by a detector scan was

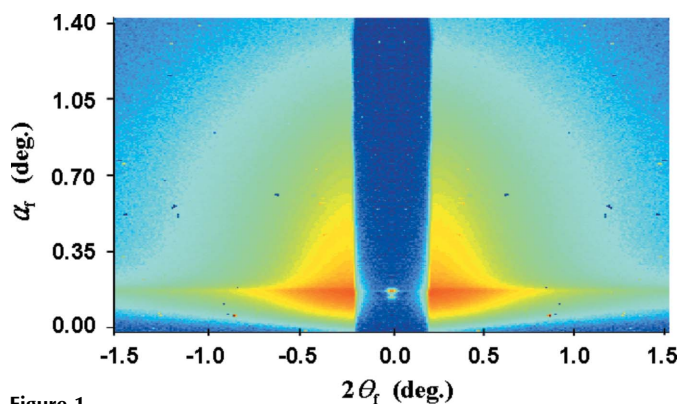


Figure 1 2D GIXS pattern measured at $\alpha_i = 0.20^\circ$ for an SiOCH film deposited with a BTMSM flow rate ratio R_{fr} of 85% and annealed at 673 K. α_i is the incident angle at which the X-ray beam impinges on the film surface; α_f and $2\theta_f$ are the exit angles of the X-ray beam with respect to the film surface and to the plane of incidence, respectively.

0.015°. The measured reflected intensities were normalized to the intensity of the incident beam, which was monitored using an ionization chamber. Ellipsometric measurements were additionally performed using a spectroscopic ellipsometer (model VASE, Woollam, Lincoln, NE).

3. Results and discussion

The SiOCH dielectrics prepared as thin films supported on silicon substrates were examined by GIXS in order to extract information on the film structure. Fig. 1 shows a representative GIXS pattern that was measured at $\alpha_i = 0.20^\circ$ for an SiOCH film deposited using a BTMSM flow rate ratio R_{fr} of 85% and annealed at 673 K. Similar two-dimensional GIXS patterns were obtained for the other dielectric films annealed at 673 K (data not shown).

From the 2D GIXS patterns measured for the films annealed at 673 K, one-dimensional (1D) in-plane and out-of-plane scattering profiles were extracted at $\alpha_f = 0.18^\circ$ and $2\theta_f = 0.27^\circ$, respectively, where α_f is the angle between the scattered beam and the film surface and $2\theta_f$ is the angle between the scattered beam and the plane of incidence. All extracted in-plane and out-of-plane scattering profiles are plotted together in Fig. 2.

We attempted to quantitatively analyze the extracted scattering intensity (I_{GIXS}) profiles using the following recently derived GIXS formula (Lee, Yoon *et al.*, 2005; Lee, Park, Yoon *et al.*, 2005; Lee, Park, Hwang *et al.*, 2005; Lee, Park, Hwang *et al.*, 2005):

$$I_{GIXS}(\alpha_f, 2\theta_f) \simeq \frac{1}{16\pi^2} \frac{1 - \exp[-2\text{Im}(q_z)d]}{2\text{Im}(q_z)} \times \left\{ |T_i T_f|^2 I_1[q_{||}, \text{Re}(q_{1,z})] + |T_i R_f|^2 I_1[q_{||}, \text{Re}(q_{2,z})] + |T_f R_i|^2 I_1[q_{||}, \text{Re}(q_{3,z})] + |R_i R_f|^2 I_1[q_{||}, \text{Re}(q_{4,z})] \right\}, \quad (1)$$

where $\text{Im}(q_z) = |\text{Im}(k_{z,f})| + |\text{Im}(k_{z,i})|$, $\text{Re}(x)$ is the real part of x , d is the film thickness, R_i and T_i are the reflected and transmitted amplitudes of the incoming X-ray beam, respectively, and R_f and T_f are the reflected and transmitted amplitudes of the outgoing X-ray beam, respectively. In addition, $q_{||} = (q_x^2 + q_y^2)^{1/2}$, $q_{1,z} = k_{z,f} - k_{z,i}$, $q_{2,z} = -k_{z,f} - k_{z,i}$, $q_{3,z} = k_{z,f} + k_{z,i}$, and $q_{4,z} = -k_{z,f} + k_{z,i}$; here, $k_{z,i}$ is the

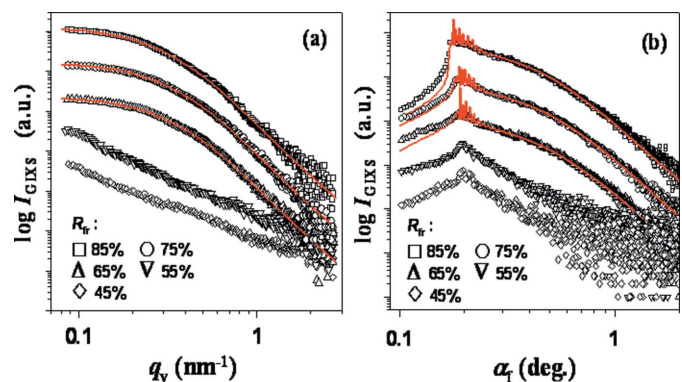


Figure 2 1D scattering profiles extracted from the 2D GIXS patterns of the SiOCH dielectric films prepared using various BTMSM flow rate ratios, R_{fr} , and subsequently annealed at 673 K: (a) in-plane scattering profiles extracted at $\alpha_f = 0.18^\circ$; (b) out-of-plane scattering profiles at $2\theta_f = 0.27^\circ$. The symbols are the experimental data and the solid lines were obtained by fitting the data with the GIXS formula for spherical scatterers.

Table 1

Pore structures and properties of nanoporous SiOCH dielectric thin films prepared from BTMSM precursor by a radio-frequency ICPCVD process.

Flow rate ratio	Annealing temperature	Pore size and size distribution			Properties		
R_{fr} (%)	(K)	r_o (nm)†	σ ‡	\bar{r} (nm)§	$\rho_{e,f}$ (nm ⁻³)¶	P_{rel} (%)††	n_R ‡‡
85	298	2.07	0.50	3.01	459	32.3	1.442
	473	2.10	0.50	3.05	456	32.7	1.441
	573	2.10	0.50	3.05	456	32.7	1.440
	673	2.11	0.50	3.07	414	38.9	1.434
75	287	1.88	0.49	2.69	514	24.2	1.443
	473	1.88	0.49	2.69	475	29.9	1.442
	573	1.92	0.49	2.75	473	30.2	1.441
	673	1.97	0.49	2.82	472	30.4	1.435
65	298	1.85	0.49	2.65	532	21.5	1.469
	473	1.86	0.49	2.66	521	23.2	1.463
	573	1.91	0.49	2.73	509	24.9	1.458
	673	1.91	0.49	2.73	505	25.5	1.448
55	298	—§§	—	—	559	17.6	1.487
	473	—	—	—	546	19.5	1.478
	573	—	—	—	538	20.6	1.473
	673	—	—	—	538	20.6	1.472
45	298	—	—	—	569	16.1	1.512
	473	—	—	—	555	18.1	1.495
	573	—	—	—	549	19.0	1.493
	673	—	—	—	549	19.0	1.486

† Pore radius determined from the peak maximum of the radius r and the number distribution of pores. ‡ Width of the radius r and the number distribution of pores. § Average pore radius determined from the radius r and the number distribution of pores. ¶ Electron density determined from the critical angle of the film. †† Porosity estimated from the electron density of the film with respect to the electron density of thermally prepared silicon oxide (678 nm⁻³). ‡‡ Refractive index measured at 633 nm using spectroscopic ellipsometry. §§ No pores were detected in the measurements.

component of the wavevector of the incoming X-ray beam, which is given by $k_{z,i} = k_o(n_R^2 - \cos^2 \alpha_i)^{1/2}$, and $k_{z,f}$ is the z component of the wavevector of the outgoing X-ray beam, which is given by $k_{z,f} = k_o(n_R^2 - \cos^2 \alpha_f)^{1/2}$, where $k_o = -2\pi/\lambda$, λ is the wavelength of the X-ray beam, n_R is the refractive index of the film given by $n_R = 1 - \delta + i\xi$ with dispersion δ and absorption ξ , α_i is the out-of-plane grazing incident angle of the incoming X-ray beam, and α_f is the out-of-plane exit angle of the outgoing X-ray beam. q_x , q_y , and q_z are the components of the scattering vector \mathbf{q} . I_1 is the scattering intensity of the structure in the film, which can be calculated kinematically.

To analyze the scattering profiles using the above GIXS formula, we examined all possible scattering models (sphere, ellipsoid, cylinder, and so on) for the I_1 term. We found that a sphere model is the most suitable for the structures in the films (*i.e.* nanopores).

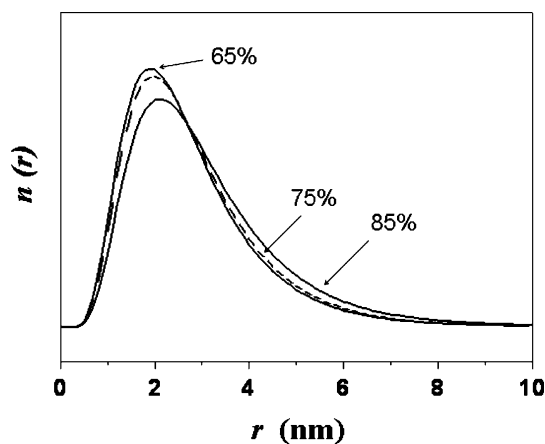


Figure 3
Pore radius distribution determined from the GIXS data analysis of an SiOCH film deposited with a BTMSM flow rate ratio of $R_{fr} = 65$ –85% and subsequently annealed at 673 K.

$$I_1 = c \int_0^\infty n(r)v(r)^2|F(qr)|^2S(qr) dr, \quad (2)$$

where c is a constant, q is the magnitude of the scattering vector \mathbf{q} , $v(r)$ is the pore volume, $F(qr)$ is the spherical form factor, and $S(qr)$ is the structure factor for the monodisperse hard sphere model (Kinning & Thomas, 1984; Pedersen, 1994). $n(r)$ is the lognormal size distribution function of the pores:

$$n(r) = \frac{1}{(2\pi)^{1/2}r_o\sigma \exp(\sigma^2/2)} \exp\{-[\ln(r/r_o)]^2/2\sigma^2\}, \quad (3)$$

where r is the pore radius, and r_o and σ are the pore radius corresponding to the peak maximum and the width of the pore radius distribution, respectively.

As can be seen in Fig. 2, the scattering profiles of the SiOCH films prepared with BTMSM flow rate ratios (R_{fr}) in the range 65–85% can be satisfactorily fitted with the GIXS formula for spherical scatterers [equations (2) and (3)]. The concordance between theory and experiment indicates that the pores generated in the SiOCH dielectric films are spherical and have a sharp interface with the dielectric matrix. For each film,

the structural parameters determined by analyzing the in-plane scattering profile were identical with those obtained from the out-of-plane scattering profile, indicating that the pores were randomly dispersed within each film.

In contrast to the films prepared using flow rate ratios $R_{fr} = 65$ –85%, the films prepared with $R_{fr} = 45\%$ and 55% exhibited featureless scattering profiles both in plane and out of plane (Fig. 2). Further, these scattering data could not be fitted with the GIXS formula for spherical, ellipsoidal, cylindrical, or disc-shaped scatterers. These observations suggest that these dielectric films did not contain any structures or pores, or that if such structures were present, they are very small.

The quantitative data analysis outlined above for the film annealed at 673 K was extended to the in-plane and out-of-plane scattering profiles extracted from the 2D GIXS patterns of the SiOCH dielectric films without and with annealing at 473 or 573 K (data not shown).

The results of the scattering data analyses of all of the films are summarized in Table 1. As can be seen in the table, the generation of pores in the SiOCH dielectric film is strongly dependent on the BTMSM flow rate ratio, R_{fr} , in the radio-frequency ICPCVD process used in this study. In the systems in which pores were detected, the pores were determined to have an average radius \bar{r} ranging from 2.65 nm for the film deposited with $R_{fr} = 65\%$ to 3.07 nm for the film deposited with $R_{fr} = 85\%$. The pore size was slightly larger in the films prepared with $R_{fr} = 85\%$ than in the films deposited with $R_{fr} = 65$ –75%. By contrast, the pore size distribution is almost the same for all of the films deposited with $R_{fr} = 65$ –85% (Table 1 and Fig. 3). Moreover, for the films deposited at a given R_{fr} condition, the pore size increased slightly with annealing temperature (Table 1). However, annealing had no effect on the pore size distribution. Overall, the present results indicate that spherical nanopores of small size ($\bar{r} = 2.65$ –3.07 nm or less) were created in the SiOCH dielectric films.

The SiOCH films were further examined by XR measurements and data analysis. Fig. 4(a) displays a representative XR profile, which

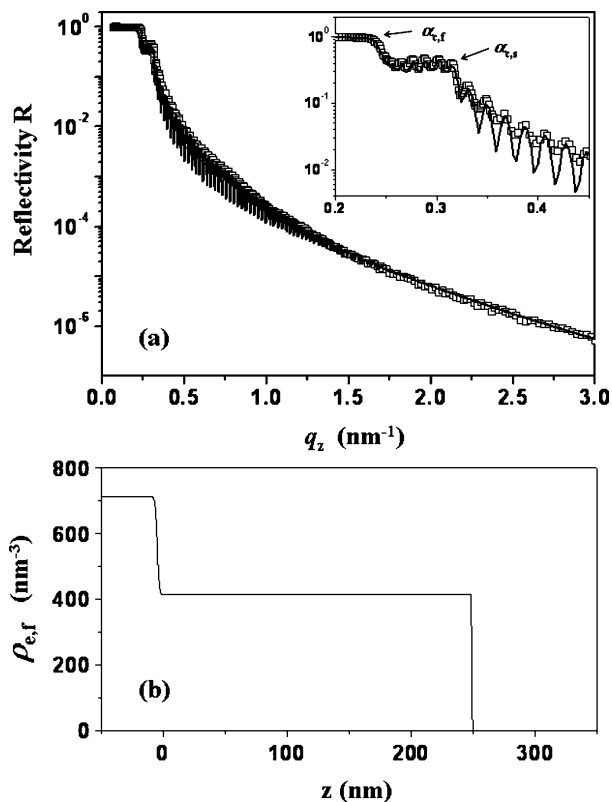


Figure 4
 (a) A representative X-ray reflectivity profile of a SiOCH film deposited with $R_{fr} = 85\%$ and subsequently annealed at 673 K. The symbols are the measured data and the solid line represents the fit curve assuming a homogeneous electron density distribution within the film except for a thin surface skin layer, in which the electron density is slightly different. The inset shows a magnification of the region around the two critical angles: $\alpha_{c,f}$ is the critical angle of the film and $\alpha_{c,s}$ is the critical angle of the Si substrate. (b) A model of the electron density distribution across the film thickness between the silicon substrate and air, which gives the best fit for the XR profile in (a).

was measured for an SiOCH film deposited with $R_{fr} = 85\%$ and subsequently annealed at 673 K. The figure clearly reveals two critical angles of the film and the substrate ($\alpha_{c,f}$ and $\alpha_{c,s}$) over the q_z range of 0.20–0.35 nm^{-1} ; here q_z is the magnitude of the scattering vector along the direction of the film thickness, which is defined by $q_z = (4\pi/\lambda) \sin \theta$, where λ is the wavelength of the X-ray beam and θ

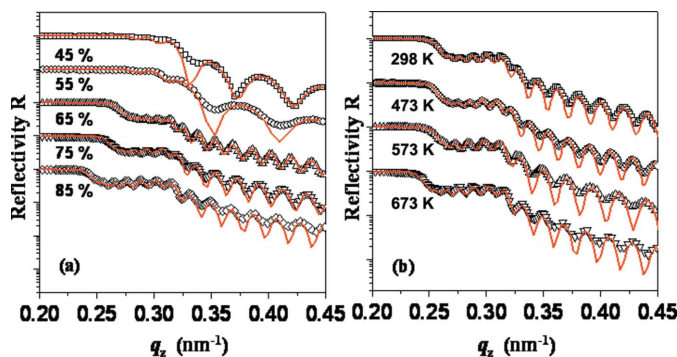


Figure 5
 (a) XR curves around the two critical angles $\alpha_{c,f}$ and $\alpha_{c,s}$ measured for the SiOCH films deposited with various BTMSM flow rate ratios (R_{fr}) and subsequently annealed at 673 K. (b) XR curves around $\alpha_{c,f}$ and $\alpha_{c,s}$ measured for the SiOCH films deposited with $R_{fr} = 85\%$ and subsequently annealed at various temperatures. The symbols are the measured data and the solid line represents the fit curve.

is the grazing-incident angle. Oscillations between the two critical angles are also clearly discernible, which are the waveguide modes for X-rays confined in the film. Thus, the reflected intensity is close to the incident one, although slightly lower due to a certain degree of absorption of X-rays in the film. Once θ exceeds the critical angle of the substrate, a significant portion of the beam penetrates into the substrate and the reflected intensity drops sharply. The steeply decaying reflectivity curve is modulated by high-frequency oscillations, which are commonly referred to as Kiessig fringes (Kiessig, 1931). These fringes appear due to interference between the beams reflected from the film–air surface and those reflected from the film–substrate interface. As the angle increases, the XR profile shows an overall decay of the reflected intensity and of the modulation amplitudes, which can be attributed to the presence of the film–substrate interface and the surface roughness.

The XR data were quantitatively analyzed using the Parratt formalism (Parratt, 1954) to obtain information on detailed structural parameters such as electron density, electron density gradient across the film thickness, surface roughness, and film thickness. As can be seen in Fig. 4(a), all features of the experimental data are well matched by the fit curve based on the Parratt formalism and a structural model (Fig. 4b) that assumes a homogeneous electron-density distribution throughout the film and a certain amount of surface roughness. It is noteworthy, however, that the minima of the Kiessig fringes are considerably shallower in the experimental data (Fig. 4a) than in the theoretical curve. The shallower depth of the minima in the experimental XR data may be associated with several factors, including a slightly inhomogeneous film thickness on the length scale of the projected beam size, curvature of the substrate induced by residual stress built up at the substrate–film interface, and so on.

The analysis provides the following structural details. The film thickness is precisely determined to be 249.4 ± 0.1 nm, and the average film electron density $\rho_{e,f}$ is 414 nm^{-3} ; here $\rho_{e,f}$ was obtained from the determined $\alpha_{c,f}$ using the relationship, $\alpha_{c,f} = \lambda \sqrt{\rho_{e,f} r_e / \pi}$, where r_e is the classical electron radius. The film surface roughness is only 0.3 nm, indicative of a very smooth surface. A very thin skin layer (0.9 nm thick) is detected, with an electron density of 356 nm^{-3} . Collectively, the XR data and analysis results indicate that a well defined structure developed in the SiOCH film deposited with $R_{fr} = 85\%$ and subsequently annealed at 673 K.

The above analysis was extended to the XR data for the other films. The findings of the analyses are summarized in Table 1, and selected XR data and the corresponding analysis results are shown in Fig. 5. Fig. 5(a) displays the XR profiles around $\alpha_{c,f}$ and $\alpha_{c,s}$ of the films deposited with BTMSM flow rate ratios (R_{fr}) of 45–85% and subsequently annealed at 673 K. All of the fits match well with the locations of the maxima and minima in the experimental data, giving a precise determination of the respective film critical angles $\alpha_{c,f}$. As R_{fr} is increased, the film critical angle $\alpha_{c,f}$ clearly decreases, indicative of a decrease in the average film electron density $\rho_{e,f}$. As can be seen in Table 1, $\rho_{e,f}$ decreases from 549 to 414 nm^{-3} as R_{fr} increases from 45 to 85%. Taking into account the finding of the GIXS analysis above that the SiOCH films deposited at $R_{fr} > 45\%$ contain nanopores, and that the nanopore number and size increase with increasing R_{fr} , we attributed the observed variations in $\rho_{e,f}$ to variations in the characteristics of the nanopores in the films. The volume of the pores (*i.e.* the relative porosity, P_{rel}) created in the films can be estimated as the $\rho_{e,f}$ values determined for the films with respect to the $\rho_{e,f}$ value for typical thermal silicon oxide, which was determined to be 678 nm^{-3} . The estimated P_{rel} values range from 19.0 to 38.9%, depending on the BTMSM flow rate ratio used in the film formation process (Table 1).

A similar trend in the variation of $\rho_{e,f}$ with BTMSM flow rate ratio was observed for the dielectric films without and with annealing treatment at other temperatures (Table 1).

Fig. 5(b) shows the XR profiles around the two critical angles, $\alpha_{c,f}$ and $\alpha_{c,s}$, for the films deposited with $R_{fr} = 85\%$ and subsequently annealed at various temperatures. As the annealing temperature is increased, $\alpha_{c,f}$ decreases, indicative of a decrease in $\rho_{e,f}$. Indeed, the value of $\rho_{e,f}$ decreases from 459 to 414 nm⁻³ as the annealing temperature is increased from 298 to 673 K (see Table 1). Taking into account the GIXS analysis results above, these variations in $\rho_{e,f}$ are again attributed to variations in the characteristics of the nanopores in the films. The volume of the pores (*i.e.* the relative porosity P_{rel}) created in the films range from 32.3 to 38.9%, depending on the annealing temperature (Table 1). In addition, the XR analysis indicated that the surface roughnesses of all of the films were in the range 0.2–0.5 nm, indicating that they had very smooth surfaces. The films were found to have a skin layer whose thickness ranges from 0.6 to 4.0 nm.

For all of the films, the refractive index n_R was measured using spectroscopic ellipsometry. The results are listed in Table 1. The films prepared with higher BTMSM flow rate ratio and annealed at higher temperature showed lower n_R values, indicative of a lower electron density.

Taken together, the GIXS, XR and ellipsometry results indicate that in the production of the porous SiOCH dielectric film by the method used here, the feed rate of BTMSM precursor is the major factor influencing the creation and final population of nanopores in the film: higher BTMSM precursor feed rates led to larger pores and higher pore populations. The pore size was slightly increased by the post thermal annealing process, with higher annealing temperatures inducing a greater size increase. Furthermore, the post-annealing process seems to either coarsen the dielectric film or generate additional pores in the film, resulting in a reduction in the electron density of the film.

The annealing-induced reduction in the film electron density might result from the chemical nature of the SiOCH film, in addition to the pores generated in the film. In the film deposition process, use of a higher proportion of BTMSM precursor in the BTMSM/O₂ flow causes an increase in the number of carbon atoms incorporated into the Si–O links, which leads to more Si–O–C bonds in the resultant SiOCH film. A high population of Si–O–C bonds in films prepared using high BTMSM precursor levels was previously identified by infrared and X-ray absorption spectroscopy (Oh *et al.*, 2004; Jun *et al.*, 2003; Yang *et al.*, 2001). The higher density of Si–O–C bonds at the expense of Si–O links serves to lower the electron density of the film. Furthermore, Si–O–C bond formation accompanied by the breaking of Si–O links might play a major role in the generation of nanopores in the film process.

4. Conclusions

A series of SiOCH dielectric thin films with nanometre-scale thicknesses were prepared by radio-frequency ICPCVD of BTMSM precursor and O₂ at various flow rate ratios and subsequent annealing at 298, 473, 573, or 673 K. The structures and properties of the resulting dielectric thin films were successfully investigated in detail by quantitative, non-destructive GIXS and XR analyses along with ellipsometry. These analyses showed that the ICPCVD of BTMSM precursor and O₂ mixtures produces high-performance low-*k* SiOCH dielectric films with a homogeneous, well defined structure and smooth surface. Moreover, the films contain nanopores and, as a

result, have electron densities and refractive indices that are much lower than those of the current workhorse dielectric, silicon dioxide. In the film formation process, a higher amount of BTMSM in the feed mix was found to produce SiOCH films with slightly larger nanopores and lower electron density and refractive index. Thermal annealing at higher temperature was found to further reduce the electron density and refractive index of the film, and to slightly increase the size of the nanopores. On average, the nanopores generated in each film were 3.07 nm in radius or less. The film electron densities ranged from 414 to 569 nm⁻³, the refractive indices ranged from 1.434 to 1.512 at 633 nm wavelength, and the porosities ranged from 16.1 to 38.9%. The characteristics of the SiOCH thin films produced in present work – homogeneous, well defined structure, smooth surface, and excellent properties – show that these films are suitable for use as low-*k* interdielectric layer materials in the fabrication of advanced ICs.

This work was supported by the National Research Laboratory (NRL) Program (Contract No. 2005-01385) and the Science Research Center (SRC) Program (Center for Integrated Molecular Systems at Postech) of the Korea Science and Engineering Foundation (KOSEF), by the Ministry of Commerce, Industry and Resources (MCIR) and the Ministry of Science and Technology (MOST) (System IC 2010 Project), by the Nuclear R&D Programs of MOST, and by the Korean Ministry of Education (Brain Korea 21 Program). Synchrotron GIXS and SXR measurements were supported by MOST and POSCO.

References

- Azooz, M. A., Hwang, Y. T. & Ree, M. (2003). *Egypt. J. Chem.* **46**, 741–756.
- Bolze, J., Kim, J., Huang, J.-Y., Rah, S., Youn, H. S., Lee, B., Shin, T. J. & Ree, M. (2002). *Macromol. Res.* **10**, 2–12.
- Bolze, J., Ree, M., Youn, H. S., Chu, S.-H. & Char, K. (2001). *Langmuir*, **17**, 6683–6691.
- Grill, A. & Patel, V. (1999). *J. Appl. Phys.* **85**, 3314–3318.
- Grill, A., Patel, V., Rodbell, K. P., Huang, E., Bakanov, M. R., Mogilnikov, K. P., Toney, M. & Kim, H.-C. (2003). *J. Appl. Phys.* **94**, 3427–3435.
- Jun, X., Yang, C. S., Jang, H. R. & Choi, C. K. (2003). *J. Electrochem. Soc.* **150**, F206–F210.
- Kiessig, H. (1931). *Ann. Phys.* **10**, 769–788.
- Kim, J.-S., Kim, H.-C., Lee, B. & Ree, M. (2005). *Polymer*, **46**, 7394–7402.
- Kim, H. J., Shao, Q. & Kim, Y.-H. (2003). *Surf. Coatings Technol.* **171**, 39–45.
- Kinning, D. J. & Thomas, E. L. (1984). *Macromolecules*, **17**, 1712–1718.
- Lee, B., Oh, W., Hwang, Y.-T., Park, Y.-H., Yoon, J., Jin, K. S., Heo, K., Kim, J., Kim, K.-W. & Ree, M. (2005). *Adv. Mater.* **17**, 696–701.
- Lee, B., Oh, W., Yoon, J., Hwang, Y., Kim, J., Landes, B. G., Quintana, J. P. & Ree, M. (2005). *Macromolecules*, **38**, 8991–8995.
- Lee, B., Park, Y.-H., Hwang, Y.-T., Oh, W., Yoon, J. & Ree, M. (2005). *Nature Mater.* **4**, 147–150.
- Lee, B., Park, I., Yoon, J., Park, S., Kim, J., Kim, K.-W., Chang, T. & Ree, M. (2005). *Macromolecules*, **38**, 4311–4323.
- Lee, B., Yoon, J., Oh, W., Hwang, Y.-T., Heo, K., Jin, K. S., Kim, J., Kim, K.-W. & Ree, M. (2005). *Macromolecules*, **38**, 3395–3405.
- Loboda, M. J., Grove, C. M. & Schneider, R. F. (1998). *J. Electrochem. Soc.* **145**, 2861–2866.
- Maex, K., Baklanov, M. R., Shamiryan, D., Iacopi, F., Brongersma, S. H. & Yanovitskaya, Z. S. (2003). *J. Appl. Phys.* **93**, 8793–8841.
- Maier, G. (2001). *Prog. Polym. Sci.* **26**, 3–65.
- Morgen, M., Ryan, E. T., Zhao, J.-H., Hu, C., Cho, T. & Ho, P. S. (2000). *Annu. Rev. Mater. Sci.* **30**, 645–680.
- Oh, K. S., Choi, C. K. & Lee, H.-J. (2004). *J. Korean Phys. Soc.* **45**, S855–S860.
- Oh, W., Hwang, Y.-T., Park, Y. H., Ree, M., Chu, S.-H., Char, K., Lee, J. K. & Kim, S. Y. (2003). *Polymer*, **44**, 2519–2527.
- Oh, W. & Ree, M. (2004). *Langmuir*, **20**, 6932–6939.
- Park, B.-J., Rah, S.-Y., Park, Y.-J. & Lee, K.-B. (1995). *Rev. Sci. Instrum.* **66**, 1722–1724.
- Parratt, L. G. (1954). *Phys. Rev.* **95**, 359–369.
- Pedersen, J. S. (1994). *J. Appl. Cryst.* **27**, 595–608.
- Ree, M. & Ko, I. S. (2005). *Phys. High Tech. (Korea)*, **14**, 2–7.
- Ree, M., Yoon, J. & Heo, K. (2006). *J. Mater. Chem.* **16**, 685–697.

- Shirafuji, T., Miyajaki, Y., Nakagami, Y., Hayashi, Y. & Nishino, S. (1999). *Jpn. J. Appl. Phys.* **38**, 4520–4526.
- Takahashi, K., Mitamura, T., Ono, K., Setsuhara, Y., Itoh, A. & Tachibana, K. (2003). *Appl. Phys. Lett.* **82**, 2476–2478.
- Yang, C. S., Oh, K. S., Ryu, J. Y., Kim, D. C., Shou-Yong, J., Choi, C. K., Lee, H.-J., Um, S. H. & Chang, H. Y. (2001). *Thin Solid Films*, **390**, 113–118.
- Yoon, J., Heo, K., Oh, W., Jin, K. S., Jin, S., Kim, J., Kim, K.-W., Chang, T. & Ree, M. (2006). *Nanotechnology*, **17**, 3490–3498.
- Yu, C.-J., Kim, J., Kim, K.-W., Kim, G.-H., Lee, H.-S., Ree, M. & Kim, K.-J. (2005). *J. Korean Vac. Soc.* **14**, 138–142.
- Yu, S., Wong, T. K. S., Hu, X. & Pita, K. (2003). *J. Electrochem. Soc.* **150**, F166–F121.